BULK AEROSOL ION CONCENTRATIONS AND THEIR IMPACTS ON TRACE METAL SOLUBILITY DURING THE US GEOTRACES GP-15 PACIFIC MERIDIONAL TRANSECT

by

DEVON UMSTEAD

(Under the Direction of Clifton Buck)

ABSTRACT

Trace elements, especially iron, are known to be limiting nutrients of phytoplankton productivity throughout much of the ocean. The GEOTRACES Prime Meridian Transect crossing the northern Pacific during Fall 2018 collected aerosol samples to measure the concentrations of aerosol major ions and trace elements. For much of the open ocean, the primary source of iron is aeolian. Acidic conditions encountered during atmospheric transport have been hypothesized to increase the solubility of iron deposited into the ocean from aerosol particles. Thus acid-forming atmospheric processes and their associated byproducts (sulfate, nitrate) may be positively correlated with iron solubility. The soluble major ions in GP-15 aerosol samples were analyzed and this hypothesis was tested by comparing those ion concentrations to the aerosol fractional iron solubility. Major ion-derived proxies were weakly correlated with aerosol iron fractional solubility, which suggests other factors drive solubility differences in the remote Pacific's low dust season.

INDEX WORDS: Aerosols, GEOTRACES, North Pacific Ocean, Trace Elements, Iron Solubility

BULK AEROSOL ION CONCENTRATIONS AND THEIR IMPACTS ON TRACE METAL SOLUBILITY DURING THE US GEOTRACES GP-15 PACIFIC MERIDIONAL TRANSECT

by

DEVON UMSTEAD

BS, University of North Carolina at Wilmington, 2015

BS, Shepherd University, 2018

A Thesis Submitted to the Graduate Faculty of The University of Georgia in Partial Fulfillment of the Requirements for the Degree

MASTER OF SCIENCE

ATHENS, GEORGIA

2022

BULK AEROSOL ION CONCENTRATIONS AND THEIR IMPACTS ON TRACE METAL SOLUBILITY DURING THE US GEOTRACES GP-15 PACIFIC MERIDIONAL TRANSECT

by

DEVON UMSTEAD

Major Professor:	Clifton Buck
Committee:	Daniel Ohnemus
	Jay Brandes
	Natalie Cohen

Electronic Version Approved:

Ron Walcott
Vice Provost for Graduate Education and Dean of the Graduate School
The University of Georgia
May 2022

ACKNOWLEDGEMENTS

I would like to acknowledge the efforts of Chris Marsay and Clifton Buck in collecting these aerosol samples and helping to guide me through the writing process.

TABLE OF CONTENTS

CHAPTER 1

INTRODUCTION

Trace metals, e.g. iron, are known to be limiting or colimiting nutrients of phytoplankton productivity throughout approximately one-third of the global ocean (Fung et al., 2000). These areas are found largely in the Southern Ocean, Central Pacific, and subarctic Northeast Pacific (de Baar et al., 1990; Kolber et al., 1994; Martin & Fitzwater, 1988). The availability of iron can determine the structure of communities, with iron-limited systems favoring smaller phytoplankton with cascading effects on the food chain and carbon capture (Fung et al., 2000; Hinckley et al., 2009). Thus, quantifying the sources, sinks, and cycling of trace metals in these regions of the ocean has become an important focus of research (Fung et al., 2000; Ginoux et al., 2001; Hamilton et al., 2020; Hand, 2004; Tagliabue et al., 2017). One example of this research effort is the international GEOTRACES project (SCOR, 2007), which aims to quantify distributions of trace elements and their isotopes through a series of transects across different ocean basins.

1.1 Aerosols

Aerosols play a key role in climate systems through numerous feedback mechanisms. Their impact on solar radiative forcing (RF), both direct and indirect, is well studied (Ginoux et al., 2001), but has major uncertainties in modern models. The most recent Intergovernmental Panel on Climate Change (IPCC, 2021) report estimates that aerosol effective RF ranges from -0.4 to -2.1 Wm^{-2}. The same report estimates the CO_2 RF as ranging from $+1.8$ to $+2.2$ Wm^{-2}.

Thus, while aerosols have a high uncertainty in forcing, they have the potential to strongly impact future climate trends.

Many aerosols scatter light in the atmosphere, directly reducing RF, with differing effects due to variations in aerosol size and composition. This scattering leads to some aerosol blocking solar radiation from reaching the earth; the estimated RF for non-absorbing sulfate aerosols ranges from −0.3 to −0.8 Wm^{-2} (IPCC, 2021). Other types of aerosols such as black soot may absorb radiation in the atmosphere, positively impacting heat budgets (Wang, 2013). The estimated RF for black and organic aerosol ranges from −0.4 to +0.4 Wm^{-2} (IPCC, 2021). Mineral dust aerosol RF is estimated between –0.04 and +0.02 Wm^{-2} but is noted to have high variability between models and is subject to active debate (IPCC, 2021; Kok et al., 2018; Schepanski, 2018). Aerosols can also serve as cloud condensation nuclei, indirectly influencing climate. Water condensing on aerosols creates clouds which can reflect and scatter solar radiation before it reaches the earth. Cloud cover and precipitation also influence climate through rain patterns and redistribution of water through the water cycle, thus impacting the climate and ecosphere (Ghan, 2013).

Aerosols have important roles in distributing nutrients and toxins from terrestrial sources, both natural and anthropogenic. Long-range atmospheric delivery is a key driver for many nutrient biogeochemical cycles in the open ocean, frequently being the dominant source of many ecologically important trace elements such as iron, copper, zinc, and manganese (Moore et al., 2013). The amount delivered that is available for biological uptake, or bioavailable, is modified by processing that occurs in the atmosphere and ocean.

Aerosols are derived from a variety of sources. Mineral dust aerosols are formed by erosion of lithogenic materials and subsequent transport into the atmosphere. This dust is formed

from the upper crustal material and is generally assumed to have the same or similar composition to that parent material. Much of this material originates from the major belts of deserts and drylands that circle the globe around 30 °N and 30 °S latitude bands. These latitude bands include arid regions such as the Sahara desert and Sahel region in northern Africa, the Arabian peninsula, central Australia, the Atacama desert and Patagonia regions in South America, and the southwest United States (Mahowald et al., 2005). Other deserts with high rates of dust emission include the Gobi Desert and the loess regions of East Asia which sit in the rain shadow of the Tibetan Plateau (Duce & Tindale, 1991). This desert is of importance to this study because of its contribution to North Pacific dust concentrations, an area of interest for studying metal limitation. Estimates of dust deposition into the North Pacific vary from 31 Mt yr^{-1} to 480 Mt yr^{-1} (Duce & Tindale, 1991; Mahowald et al., 2005; Zender, 2003). Climate change, land use changes, and weather patterns influence annual variability of dust deposition to the North Pacific. Many questions remain as to the overall trends on decadal and climatic timescales (Guo et al., 2019)

Aerosols are also derived from anthropogenic activity, including the burning of coal, oil, gasoline, and biomass. These pyrogenic aerosols are very different chemically and physically from mineral dust. They contain a higher concentration of a variety of heavy metals which are able to be released into the water column and contribute to total marine pollution levels (Fitzgerald, 1991). Multiple areas of study for the influence of these aerosols exist, with focus on the North Atlantic and Northwest Pacific due to their proximity to heavily industrial human population centers.

Sea salt aerosols (SSA) are formed by the action of winds and waves ejecting small particles of water. The ejection can occur in a variety of ways. Bubbles entrained in the surface

waters by the actions of waves can burst and eject SSA into the atmosphere. At higher wind speeds, SSA can be sheared off the surface of waves. Once in the atmosphere, these aerosols contribute to the total aerosol loading and can be transformed by the interaction with trace gases, photochemistry, other aerosols, and drying.

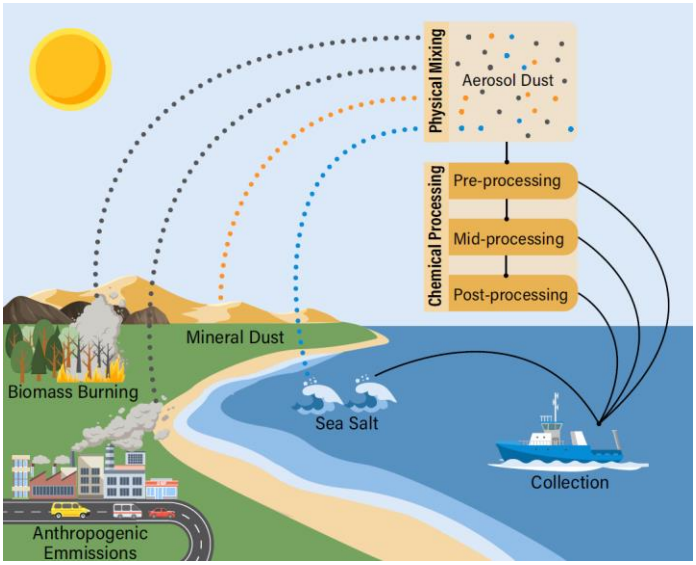

Figure 1 Schematic diagram of the aerosol collection process. Aerosols are collected from their primary sources after being physically mixed and chemically processed in the atmosphere. Different factors will determine how much processing is done to each aerosol. Sea salt aerosols are generated much closer to collection and may be unmixed and unprocessed.

There are several other processes that produce aerosols that are important on different spatial and temporal scales. Volcanic activity can inject significant aerosol amounts, sufficient to affect global climate. Volcanic ash is also enriched in iron (Stewart et al., 2006), but due to the stochastic nature of volcanic eruptions, quantifying total inputs within a given timescale is difficult. While some of the global pyrogenic biomass is anthropogenic, natural forest fires and scrubland fires contribute to total aerosol loading and aerosol trace elements (Alves et al., 2010), with one study recording as high as 20% of total natural emissions for Zn (Echalar et al., 1995). This study also notes the large chemical differences between scrubland-derived aerosols and forest fire-derived aerosols, which are an important factor in the spatial scales of natural pyrogenic aerosol generation (Echalar et al., 1995; Kelly et al., 2021). Marine areas downwind of different terrestrial ecosystems will receive varying amounts of trace elements depending on the dominant plant-life, which may also be influenced by a changing climate.

1.2 Trace Metals

For much of the open ocean, atmospheric deposition is the primary source of trace metals (Buck et al., 2019; Duce & Tindale, 1991; Pavia et al., 2020). These aerosols originate from a variety of sources and contain variable amounts of iron and other metals. Likewise, these metals will also have different fractional solubilities (defined as the percentage of the total aerosol trace element that dissolves in a solution; see section 3.6) depending on their source and atmospheric processing prior to deposition (Ito & Shi, 2016). Estimates of aerosol iron solubility and chemical speciation range widely, with different methodologies giving a wide range of results (Perron et al., 2020). Literature values of aerosol Fe solubility range from 0.01% to 90% (Baker & Croot, 2010; Mahowald et al., 2005; Perron et al., 2020). The chemical partitioning processes that determine dissolvable iron concentrations after marine deposition are complex and difficult to constrain (Baker & Croot, 2010; Buck et al., 2013) and partly depend on the source material and atmospheric processing before deposition. Previous work has hypothesized that acidic conditions encountered during atmospheric transport to the deposition location may increase aerosol iron solubility (Baker et al., 2021; Buck et al., 2006; Chester et al., 1993; Duce & Tindale, 1991). If this is true, then it follows that acid-forming atmospheric processes and their associated byproducts (sulfate, nitrate) may be positively correlated with iron solubility.

Upper continental crust is generally rich in iron (3.5%) (Taylor & McLennan, 1995). Iron is commonly found in minerals such as magnetite, wüstite, and hematite. However, these minerals are generally insoluble in seawater (fractional solubility less than 1%) (Labatut et al., 2014; Spokes & Jickells, 1995), though exceptions exist (Buck et al., 2010). Another source of marine aerosols is derived from anthropogenic and pyrogenic emissions, largely from combustion sources (Conway et al., 2019). These sources show higher iron solubility (often

greater than 50%), with petroleum combustion by-products specifically having a fractional solubility of up to 81% (Ito et al., 2019; Perron et al., 2020; Sholkovitz et al., 2012). Thus, despite the low relative concentration of pyrogenic aerosols when compared to mineral dust aerosols globally, the former is likely to be an outsized source of dissolvable iron to much of the open ocean. One recent report suggests that anthropogenic Fe contributes 21–59% of dissolved Fe measured between 35 °N and 40 °N in the Pacific (Pinedo-González et al., 2020).

Pyrogenic aerosols are suggested to contain more iron per particle and iron in more soluble forms than iron present in mineral dust for several reasons. Particles derived from pyrogenesis are typically smaller than dust particles (Damle et al., 1981), which gives them a higher surface area to volume ratio. A higher surface area to volume ratio allows for more of the particle to be in contact with seawater, increasing the rate of dissolution and reactions with constituents of ocean water, such as ligands. Aerosol iron speciation also differs between pyrogenic and mineral sources. Mineral iron is typically found bound to oxides that are largely insoluble, while pyrogenic iron is found in the form of ferric sulfides and sulfates which are more soluble (Ito et al., 2019; Li et al., 2017).

An additional factor is the changing composition of the atmosphere, especially particle pH and pe^-, due to anthropogenic inputs of acid-forming species. Iron and many other metals are more soluble at lower pH and are impacted by these compositional changes (Ito & Shi, 2016). These chemical factors change over different temporal and spatial scales, varying with seasonal emission patterns and with distance from land. Because of the limitations of aerosol sampling, only the concentration of aerosols and their composition is measured directly. The relative amount of atmospheric processing may be inferred from observed correlations found among the constituent chemical components. Ultimately, because of these factors, the assessments of

bioavailability of aerosol iron are uncertain and parameterizing the difference in sources is a key research aim.

Because iron is relatively insoluble in modern marine systems, organisms have evolved different strategies to obtain iron from seawater (Hutchins et al., 1999). For example, many organisms excrete iron-binding ligands called siderophores to bind and transport iron into their cells (Amor et al., 2020). Bioavailability is difficult to directly assess chemically, thus we frequently assume that dissolved iron is bioavailable, while particulate iron is not. However, the phytoplankton communities have diverse uptake mechanisms and have been seen taking iron from non-dissolved phases (as operationally defined as iron which passes through a 0.2 μm filter for this study) including large biomolecules (Shaked & Lis, 2012; Sutak et al., 2020) and solid dust particles (Kessler et al., 2020). Biological access to particulate trace elements is also poorly constrained (Hutchins & Bruland, 1994; Shaked & Lis, 2012). Traditional laboratory experiments typically only measure the total aerosol trace metal concentrations (by treatment with hydrochloric acid, nitric acid, hydrogen peroxide, and hydrofluoric acid) and measure aerosol solubility in one of ultrapure water (>18 MΩ·cm), seawater, or a variety of pH or redox modified solutions (Perron et al., 2020). While there are many chemical procedures used to measure bioavailable trace elements (see Perron et al., 2020), none of them perfectly represent the fraction of the aerosol trace metals ultimately available for biological use. As with the macronutrients nitrogen and phosphorus, biological processes are a major component of trace element biogeochemical cycles. Determining what processes increase bioavailability of these trace elements is a key goal to understanding the cycling of these elements and what changes may occur with increasing human impact to the global oceans.

1.3 Atmospheric Processing

One of the primary methods of atmospheric aerosol processing is cloud formation. Cloud formation involves the condensation of water onto appropriate nuclei, called cloud condensation nuclei (CCN). Both the physical aspects of the aerosol particles, such as size and shape, and the chemical traits, such as hydrophobicity and solubility of the aerosol, affect its ability to serve as effective CCN. As these aerosols begin to form clouds, they will also interact with water, which can change the reactions that occur at the aerosol surface.

Liberation of acid- and base-forming species can create or accelerate a variety of complex chemical interactions (Baker et al., 2021; Chen et al., 2011; Paris & Desboeufs, 2013). One of the better studied reactions is an acid-base reaction between sulfuric acid and chloride anions. This reaction creates dissolved or gaseous hydrogen chloride (HCl). In the gas phase, HCl can escape aerosols, in a process called chloride depletion. This process can decrease overall acidity by removing hydrogen ions from particles, but not all models of acidity account for chloride depletion (Baker et al., 2021; Buck et al., 2010) and HCl may react with other aerosols as a trace gas to reintroduce hydrogen ions. However, like many of the other reactions, the constraints are unknown, and trends are assumed from the correlations found in nature. Aerosol properties may also change during transport due to aging processes such as participation in ice formation or chemical reactions with other aerosols and atmospheric chemicals (Schepanski, 2018).

1.4 Study Background

The sampling area of the 2018 U.S. GEOTRACES GP15 Pacific Meridional Transect (PMT) cruise crosses a diverse set of biogeochemical and climatic regimes, ranging from the sub-Arctic Gulf of Alaska to the equatorial South Pacific. The Gulf of Alaska (GoA) has long been hypothesized to be limited by iron (Martin & Fitzwater, 1988) and is a region of active

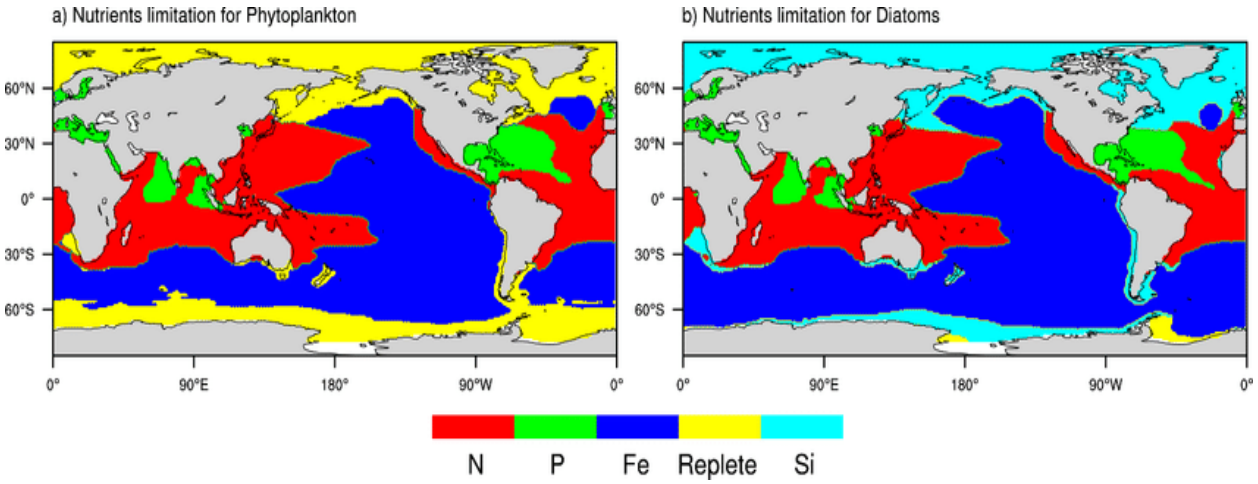

Figure 2 Global nutrient limitation patterns for Diatom and other phytoplankton — from Dai et. al. (2019). This figure shows a global model of regions where organisms are limited by specific nutrients. Throughout most of the study area, iron is the limiting nutrient for both diatoms and other phytoplankton.

research on iron's role in ecosystem structure (Coyle et al., 2019; Hinckley et al., 2009). The GoA is marked by storms, which influences aerosol origin, composition, and amount, heavily favoring larger amounts of local sea spray injection to the atmosphere. Southward towards the temperate central Pacific, the weather becomes calmer; this region of the transect is found under the subtropical high-pressure zone – an area of low precipitation and humidity, with decreased favorability for sea spray aerosol creation. The central and subtropical Pacific are oligotrophic, primary production is limited by low nutrient concentrations. At the equator, upwelling creates an environment enriched in nitrogen and phosphorus relative to the nearby areas (Kolber et al., 1994). This area is also where the intertropical convergence zone (ITCZ) lies. The ITCZ is a seasonally migratory band of high rainfall that lies at the convergence of the trade winds. South

of the equator, oligotrophic conditions return as the route enters the subtropical South Pacific gyre.

Figure 2 presents a global model of ocean nutrient limitation with a focus on the area of the GP15 transect presented here (Dai et al., 2019). Other than the near shore areas to the immediate south of Alaska, the entire transect is limited by iron for both diatoms and other phytoplankton in this model. Incubation studies of phytoplankton communities in the region of the transect also support the model results (Moore et al., 2013). Alaskan coastal regions are limited primarily by silica for diatoms. Other phytoplankton populations in the coastal portions of the transect labeled as replete are either limited by sunlight, space, are controlled top-down by predation or non-chemical factors.

The abundance of major aerosol ions (Na^+, Ca^{2+}, Mg^{2+}, Cl^-, SO_4^{2-}, and NO_3^-) can help constrain the portion of that are autochthonous (largely in the form SSA), combustion byproducts, or from natural mineral sources. Because the major ions, with the exception of nitrate, are conservative in ocean waters, those ions should have a consistent ratio if they are derived from oceanic spray. Sulfate is found both in seawater and as a byproduct of other aerosol-producing processes like fossil fuel combustion. The ratio of aerosol sulfate and sodium relative to the marine ratio can be used to differentiate sea spray aerosols from aerosols derived from other processes that are typically enriched in sulfur, i.e., non-sea salt sulfate (nss-sulfate). Sulfur released from anthropogenic processes typically comes in the form of sulfur dioxide that can be oxidized into sulfuric acid by the action of oxygen radicals and water in the atmosphere, thus lowering the pH of aerosols. The ratios of the major ions can also be used to determine the potential mineral loading relative to local sea spray input. Measuring these ions also allows for

quantification of nitrate delivery over the sampling area (Buck et al., 2006), including the oligotrophic North Pacific gyre which is co-limited by nitrogen (Moore et al., 2013).

Because of iron's key role in the limitation of primary production, its bioavailability and sources are important topics of research within chemical oceanography. Desertification as a consequence of climate change and land use changes are predicted to increase mineral trace elements reaching the ocean (IPCC, 2021), though observational verification is lacking for the North Pacific (Guo et al., 2019; Zhao et al., 2006). Industrialization of eastern Asia has led to increased release of acid producing sulfur and nitrogen species and pyrogenic iron (Guo et al., 2019; Ito & Shi, 2016; Pinedo-González et al., 2020) which will interact with potential changes in mineral dust loading due to climate change. Potential increases to total deposited iron and iron solubility will have impacts on the ecology and carbon cycling within this region and beyond (Hamilton et al., 2020; Pinedo-González et al., 2020; Winckler et al., 2016). Constraining the sources of bioavailable trace metals to the ocean, especially in metal-limited areas, is essential for understanding the processes that underlie the linkages of these important global issues.

CHAPTER 2
METHODS

2.1 Cruise Information

The U.S. GEOTRACES GP15 Pacific Meridional Transect (PMT) ran between Alaska and Tahiti, roughly tracing the 152 °W meridian between 56 °N and 20 °S (Fig. 2). The cruise took place between September 18th and November 24th, 2018, aboard the *R/V Roger Revelle*. As with all GEOTRACES cruises, this project supported scientists and teams with individual projects related to the central goal of quantifying and studying the biogeochemical cycling of trace elements and their isotopes in both the ocean and near-ocean atmosphere, including aerosols.

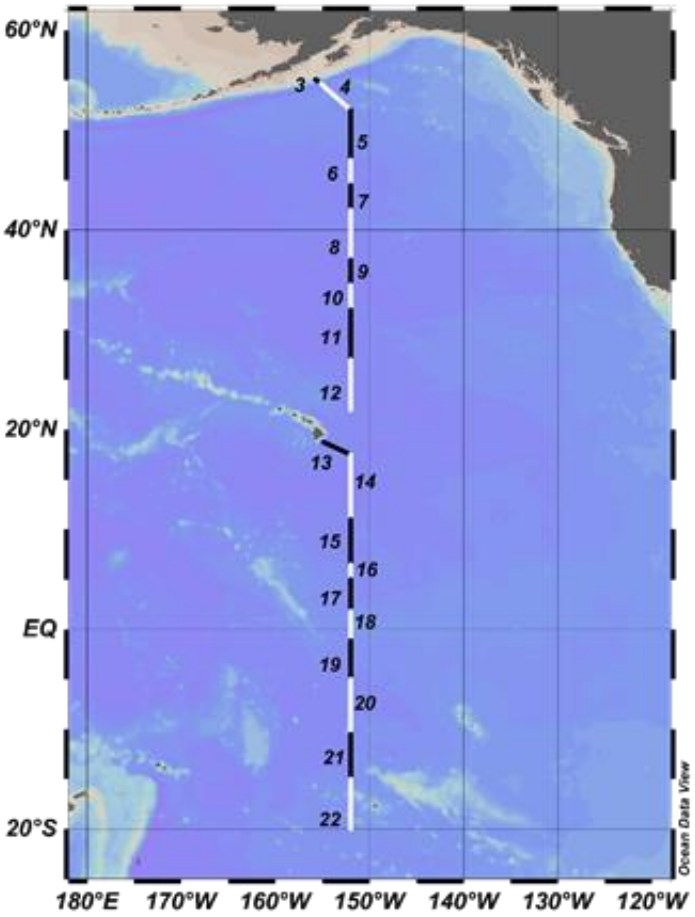

Figure 3 Track of the GEOTRACES GP15 cruise showing the two legs of the trip between Alaska and Hawaii, and Hawaii and Tahiti. Aerosol collections are indicated by numbers while the length of the line segment indicates the region covered by each collection. Odd numbered collections are indicated by black segments and even numbered collections are shown with white segments.

2.2 Sample Collection

During GP15, Skidaway Institute scientists collected 23 bulk aerosol samples. One deployment was canceled due to rough seas while in the GoA. Samples were collected using high volume aerosol samplers (1.2 m^3 air min^{-1}; Tisch Environmental, model 5170V-BL) that

were deployed on the forward rail of the *R/V Roger Revelle's* 03 deck, about 16 m above the ocean. To prevent ship exhaust from contaminating the samples, sampling was restricted to periods when the relative wind direction and speed were ±90° of the ship's bow and >0.5 m s^{-1}, respectively, as measured by an anemometer and wind vane interfaced with the samplers through a Campbell Scientific CR800 data-logger. These deployments averaged 40 hours of total sampling time carried out over 1 to 4 days. The mean air volume sampled through each filter was 240 m^3. On each deployment, 12 replicate acid-washed 47 mm Whatman 41 ashless filters were mounted on polypropylene filter holders (Advantec-MFS) and installed on the aerosol sampler upon a custom-built polyvinyl chloride adaptor plate. The filter manipulation was all done inside of a plastic "bubble" that was constructed in the ship's main laboratory. HEPA-filtered air was supplied to the "bubble". All filters were handled with acid-washed tweezers.

Figure 4 A Tisch Environmental bulk aerosol sampler shown with the vacuum motor exposed.

Figure 5 A custom adapter provides 12 replicate samples from each Tisch aerosol collector.

2.3 Sample Processing and Analyses

Following sampling, the filters were transfer to pre-labeled petri slides. A set of filters from each deployment were "instantaneously" leached with ultrahigh purity (>18 MΩ·cm; UHP) water according to the methods in previous studies (Buck et al., 2006; Morton et al., 2013). Other filters were transferred to petri-slides and stored frozen until trace element processing back on land. Approximately 30 mL from each leach was collected in an LDPE bottle to serve as a subsample to be analyzed for major ions. This subsample was stored frozen in a commercial freezer until analysis.

The concentration of the major cations and anions were analyzed by ion chromatography (IC) on a Dionex ICS-2100 instrument. Target analytes were Na^+, Ca^{2+}, Mg^{2+}, Cl^-, SO_4^{2-}, and NO_3^-. The concentrations of the ions were calculated by linear regression of the system response to a series of standards of known concentration. Analytical accuracy was confirmed by regular analysis of check standards. All standards were made with ACS certified salts in UHP. Ion concentrations for each collection were normalized to pmol m^{-3} by dividing by the volume of air sampled.

The analytical uncertainty was assessed by measuring six samples in triplicate (the highest, the lowest, and four random samples) and obtaining the mean, standard deviation, and the relative standard deviation (RSD) of each triplicate. The RSD for all six samples were averaged for each analyte to get a mean RSD for each individual analyte, which is expressed as a percentage of the total concentration.

The bulk aerosol iron analysis has been described in Marsay et al (2022) in full and is consistent with protocols from previous U.S. GEOTRACES cruises and other program cruises (Buck et al., 2019; Buck et al., 2013; Buck et al., 2010; Marsay et al., 2022). Briefly, the frozen filters were treated with a three-step strong acid digestion protocol (Morton et al., 2013) in a Class-100 clean room facility at Skidaway Institute of Oceanography. Each filter was placed in a 15 mL perfluoroalkoxy (PFA; Savillex) digested at 140 °C with double distilled nitric acid, concentrated hydrofluoric acid (Fisher Trace Metal Grade), and concentrated hydrogen peroxide (Fisher Optima Grade). Residues from the filters were dissolved in 0.32 M distilled nitric acid for analysis. Unused Whatman 41 filters were treated in the same way to obtain blank values. The same treatment was used to digest small quantities of MESS-3 marine sediment certified reference material (National Research Council of Canada) and the Arizona Test Dust community reference material to evaluate the efficacy of the procedure.

We measured Al, Ti, V, Cr, Mn, Fe, Co, Ni, Cu, Zn, and Pb in the samples, blanks, and reference material by inductively coupled plasma mass spectroscopy (ICP-MS; Perkin Elmer NexION 300D), using a seaFAST S2 system in Direct Mode (Elemental Scientific Inc.). Samples were analyzed alongside external standards prepared in 0.32 M nitric acid from multielement and single element solutions (Inorganic Ventures). Measured trace element concentrations were

converted to picomoles per digest, blank corrected by subtracting the mean digestion blank, then normalized to pmol m^{-3} by dividing by the volume of air sampled.

We measured UHP-soluble iron fractional solubility using a method developed in prior studies (Buck et al., 2006; Morton et al., 2013). Sample leaching was conducted using a Nalgene polycarbonate filtration rig. The ‘‘instantaneous’’ solubility of Fe in UHP water was measured by quickly passing 100 mL with unacidified DI water (pH 5.6) through one 47 mm aerosol filter. The water was poured into the filtration rig while a vacuum was applied using a small pump. The filtration was completed within 10 seconds. We then measured the iron in the filtrate. Fractional solubility was calculated as the concentration of soluble iron divided by the total digest iron (see section 3.6)

2.4 Back Trajectory Analyses

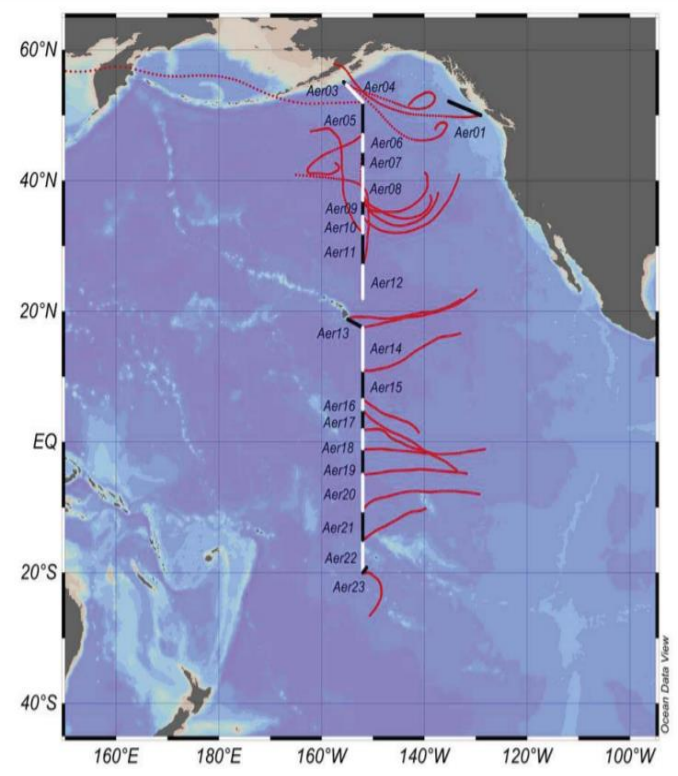

Figure 6 HYSPLIT modelled back trajectories of all samplings. Note only one station had air that had encountered land in the prior three days.

Back-trajectories of air masses passing through each aerosol sample deployment and recovery location were modelled with the internet version of the NOAA Air Resources Laboratory Hybrid Single-Particle Lagrangian Integrated Trajectory (HYSPLIT) model (Rolph et al., 2017; Stein et al., 2015). Global Data Assimilation System (GDAS) meteorology data at a 1º latitude resolution was used to simulate five-day (120 h) air mass back trajectories (AMBTs) in ensemble mode. This

provides several trajectories by offsetting the meteorological data by a fixed grid factor. An arrival height of 250 m was used because the model is not well suited for arrival heights within the marine boundary layer. However, several test cases were run with the arrival height set to the elevation of the samplers and no significant differences were found in the modeled trajectories. Single trajectory, three-day AMBTs were also produced to overlay on the cruise track in Figure 6, and additional ten-day HYSPLIT runs were performed to extend AMBTs further back in time, however model uncertainty increases with each timestep.

CHAPTER 3

RESULTS AND DISCUSSION

3.1 Sodium

Soluble aerosol sodium concentrations are highest in the northern portion of the transect corresponding to the Gulf of Alaska and the temperate northern Pacific under the influence of the westerlies. The concentrations decrease into the subtropical and tropical North Pacific corresponding to the subtropical ridge – an area of high atmospheric pressure with lower wind speed and wave height. Concentrations again increase upon entering the windier areas influenced by the trade winds and the ITCZ, before decreasing for the final two stations on the southern side of the ITCZ.

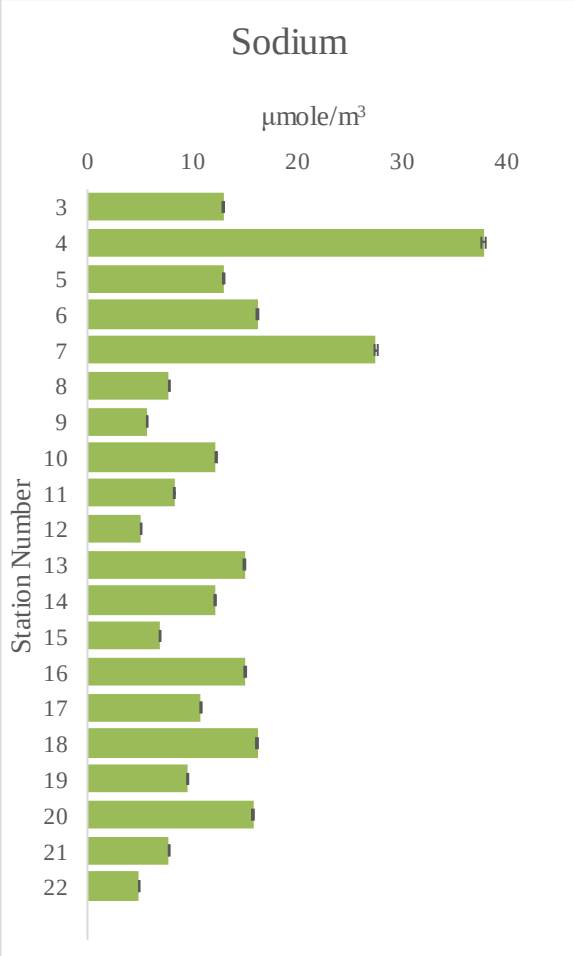

Figure 7 Sodium ion concentrations across the transect. The station number geographic locations are given in figure 3. The error bars represent a percentage RSD – 0.55%

Sodium is the most representative of sea salt contribution of the cations measured here. While sodium is not rare in crustal materials (2.9% of upper crustal mass by weight (Taylor & McLennan, 1995)), mineral sodium is much less soluble than marine-derived sodium. Many of the common sodium-containing terrestrially derived

minerals, such as albite feldspars, are insoluble. On this transect, sea salt sodium is far more abundant relative to the mineral sodium contribution. This potential contribution has been calculated previously using observed Ti values, and results in SSA Na having >100x the mineral Na contribution to the total in most samples (Marsay, in review). Thus, there is no correction for terrestrially derived sodium needed when using sodium as a proxy for seawater to calculate the non-sea salt contribution of various ions.

3.2 Magnesium and Calcium

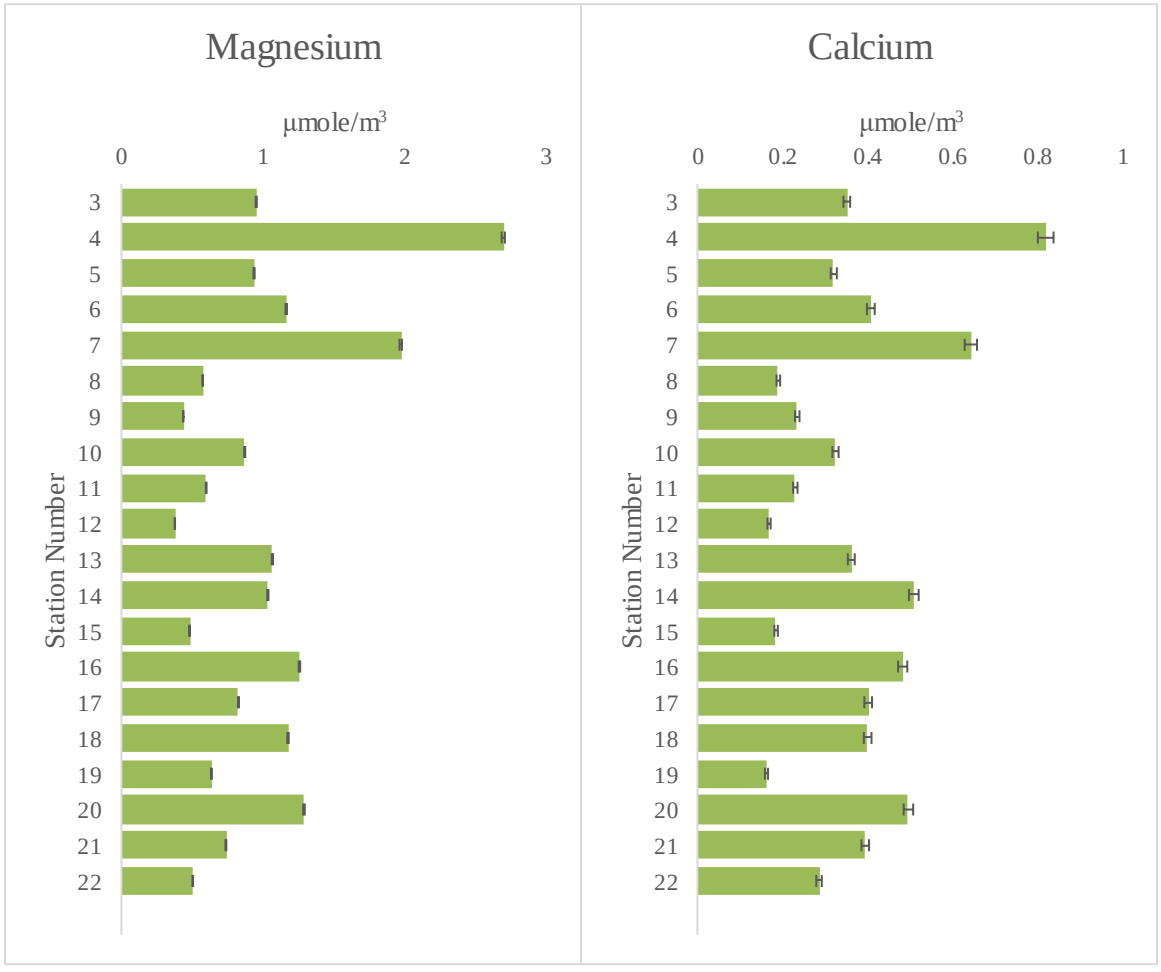

Figure 8a-b Magnesium and calcium concentrations found during the transect. The error bars represent an average percentage relative standard deviation – 0.44% for Mg, 2.25% for Ca

Magnesium and calcium are two other conservative cation species found in SSA. They grossly follow the same pattern as sodium. Each is highest in the northern portions of the

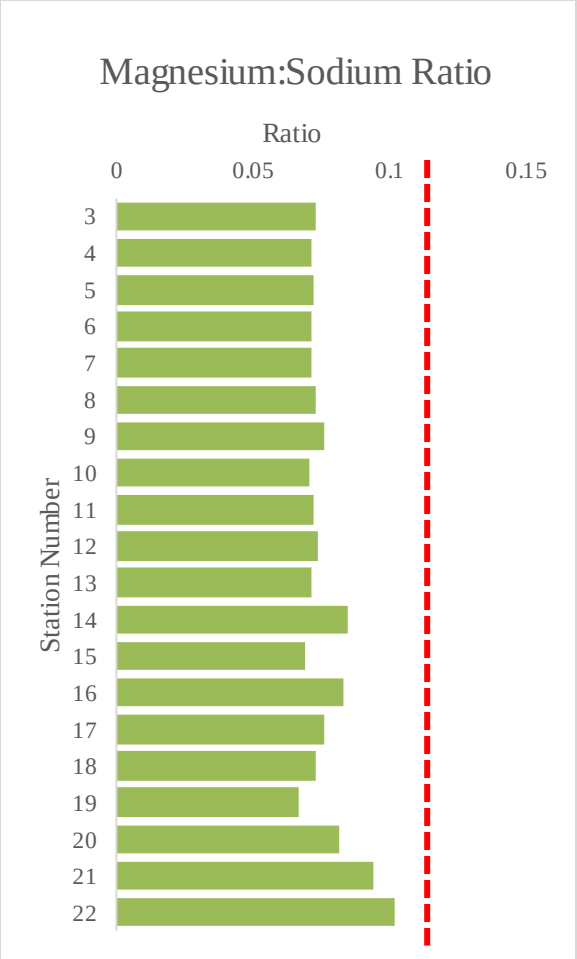

Figure 9 The ratio of magnesium to sodium at each station. The dashed line marks the oceanic Mg:Na ratio (0.11).

transects in the North Pacific, decrease in the subtropical and tropical regions, then increase again in the area influenced by the ITCZ. Magnesium and calcium concentrations can serve as a useful quality control check by comparing their respective ratios to sodium with those of other major ions. Internal ratios of the solely sea salt-derived ions are largely consistent ($\bar{x} = 0.076$, $\sigma = 0.008$; Figure 9). This result suggests that these ions are derived from the same sources. Some of the assumptions made about the leeching process are also confirmed here – specifically that there are little readily soluble mineral forms of the selected ions in these samples.

The Mg:Na ratio was also found to consistently be less than the ratio found in seawater (0.11; dashed red line in Figure 9). This deviation has been found in a previous study as well (McInnes et al., 1994). The reasoning for this observation is not definitive, but may be an artifact of sampling or leaching methods. When seasalt aerosols are dried upon ejection from the ocean, the soluble ions dry into a variety of salts with varying degrees of hydration. Some of these salts are not readily soluble and may be missed by an instaneous leach, including calcium and magnesium carbonates (calcite and dolomite), sulfates (gypsum and kieserite), and hydroxides (brucite and lime). These minerals can also interact with the atmosphere to form secondary products (calcium and magnesium oxides) in

specific conditions of heat, humidity, and by reactions with trace gasses. These secondary products are frequently poorly soluble as well. Thus, the instantaneous leach used in this study may not capture elements locked in these secondary minerals.

3.3 Chloride

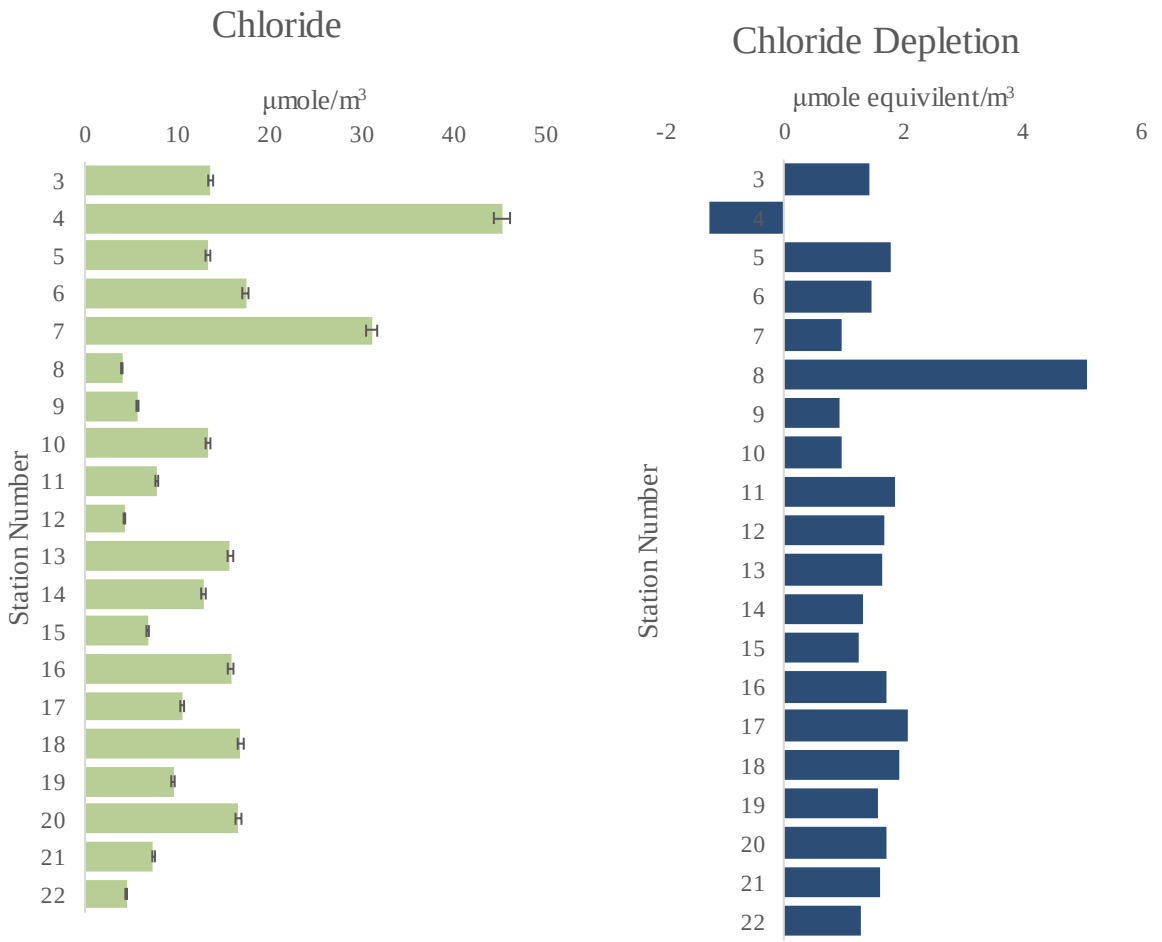

Figure 10a-b a) Concentrations of aerosol chloride found along the transect. The percentage RSD was 1.95% b) Chloride depletion along the transect. The method found in Mukherjee et al (2022) was used to calculate chloride depletion, exchanging weight ratios for molar ratios.

Chloride also follows a similar pattern to the major cations. Aerosol concentrations peak at the northern section of the transect, between stations 4 and 7, followed by an immediate low through the central North Pacific. Afterwards, concentrations increase again in the central Pacific before decreasing towards the end of the transect south of the equator.

Eq 1: $Chloride\ Depletion = 1.16 * [Na^+] - [Cl^-]$

Chloride can also participate in gas phase chemistry by the acceptance of a proton to form HCl. This process is called chloride depletion. The proton accepted may come from sulfur or nitrogen oxidation, and the HCl produced can participate in aerosol-gas chemistry. This is discussed in further detail in section 3.6. The HCl generated from this process can also react with other aerosols to enrich them in chloride and lower their pH or be deposited as dry HCl onto samples or the open ocean (McInnes et al., 1994).

3.4 Sulfate and nss-Sulfate

Figure 11 a-b a) Concentrations of aerosol sulfate found along the transect - RSD 2.73%, b) The percentage of the total sulfate that was derived from nss-sulfate sources.

Like the other analytes presented here, sulfate follows much of the same pattern geographically. These sulfate concentrations were used to calculate the non-seasalt sulfate (nss-sulfate) of the aerosols sampled. The concentration of nss-sulfate was calculated using equation 1. The marine [Sulfate] and marine [Sodium] values are based on the marine molar ratios of sulfate and sodium in the ocean (equal to 0.06), while the [Sulfate] and [Sodium] terms are the measured concentrations of sulfate and sodium in each sample.

$$\text{Eq 2: } [nss\text{—}Sulfate] = [Sulfate] - \left(\left(\frac{Marine\,[Sulfate]}{Marine\,[Sodium]}\right) * [Sodium]\right)$$

Of interest, the percentage of total sulfate that is derived from nss-sulfate varies in a slightly different pattern. Station 4 had the lowest percentage of sulfate being derived from nss-sulfate at 6%, while station 21 had the most at 54%. The ITCZ influenced area and the southern edge of the transect are laden with more nss-sulfate than the remainder of the transect. This section of the transect includes areas of high aerosol transport. The nss-sulfate in this area may also be derived via oxidation of dimethyl sulfone or other sulfur containing compounds released by marine organisms in the highly productive equatorial Pacific (Fitzgerald, 1991; Ghahremaninezhad et al., 2016). The oxidation pathway for these sources of sulfur still forms sulfuric acid and contributes to the acidity of the aerosol environment. So, while this will influence the chemical relationships one would expect, it does not change the way acidity needs to be calculated.

3.5 Nitrate

Aerosol nitrate concentrations vary along the transect in a different pattern than the other analytes, which is suggestive of its different sources. Concentrations are highest at the stations north of 40 °N. The concentrations of nitrate decline in the subtropical and northernmost sections

of the tropics, with a small decline at 18 °N. The areas south of the ITCZ have a considerably lower concentration of aerosol nitrate.

Nitrate has multiple sources, some unique from the other analytes presented here. Nitrate is a common byproduct of combustion processes, typically formed in the oxidation of the various nitrogen oxides (NO_x) or release of incompletely oxidized NO_x species that can be further oxidized in the atmosphere. Lightning can also produce NO_x by the reaction of atmospheric oxygen and nitrogen. Biota can also produce N_2O and other gaseous nitrogen species through denitrification. N_2O and NO_x can ultimately form nitrate by the oxidizing actions of oxide and hydroxide radicals in the atmosphere. Ammonia released during the fertilization of farmland or industrial processes can also be oxidized in the atmosphere to nitrate and attach to aerosols.

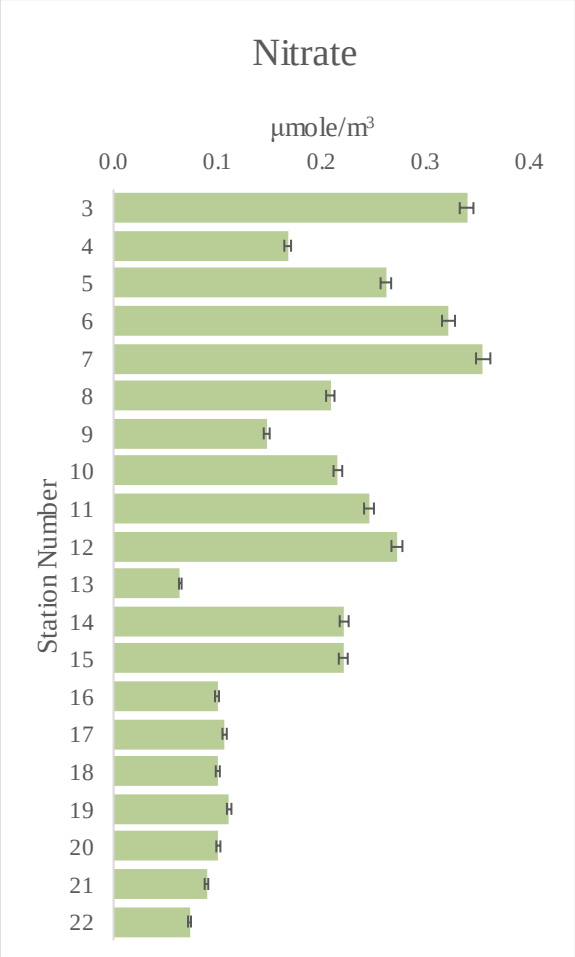

Figure 12 Concentration of nitrate along the sample transect. Nitrate RSD – 1.06%

Aerosol tracing methods including sulfur and nitrogen isotopic analysis and matching with other proxies gathered during oceanic sampling projects can be used to discuss how these aerosols are sourced. Many of the previously listed nitrate sources have very distinct isotopic signatures (especially denitrification). If the sources of sulfate and nitrate are found to be locally derived, then this may explain the unexpectedly low

correlation between iron solubility and acid forming species, as the iron-bearing aerosols may not have been exposed to the acidic environment during transport.

3.6 Aerosol Acidity

Aerosol acidity was calculated according to Equation 2. The concentration of nss-sulfate was calculated according to Equation 1 earlier and [Nitrate] is the measured concentration of aerosol nitrate in the samples. The nss-sulfate concentration is multiplied by two because sulfate can donate two protons to solution at common pH values. This equation has been used in prior studies (Buck et al., 2006).

Eq 3: $Acidity = 2 * [nss - Sulfate] + [Nitrate]$

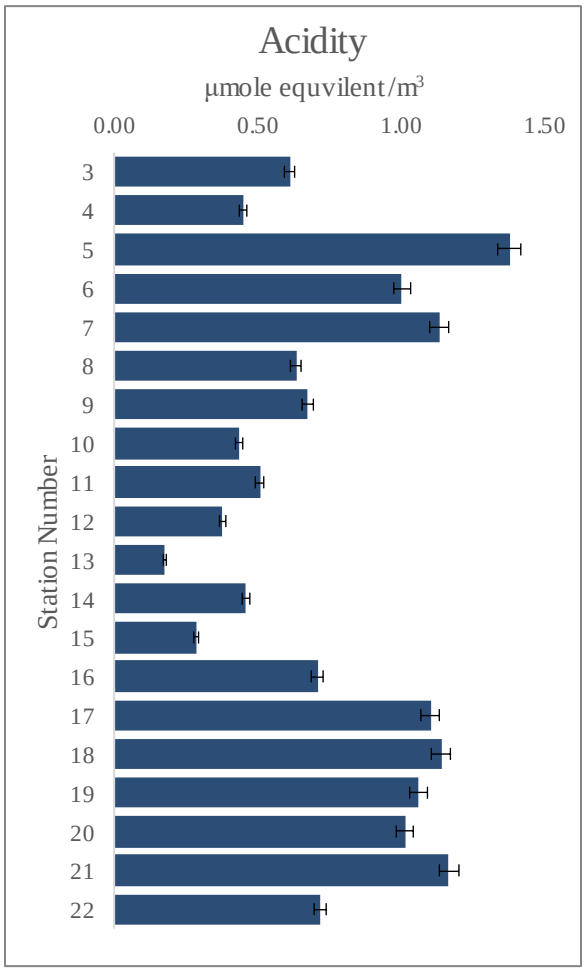

Figure 13 Acidity molar equivalent for each station. The RSD as calculated by error propagation was 2.93%.

Acidity concentrations vary in a similar, but not identical, pattern to the major ions along the transect. There is a minimum in station 13 near Hawaii, and the peak occurs at station 5 (unlike the major ions, where the peak is at station 4). The values range over an order of magnitude — between 1.38 and 0.18 µmole equivalent of acid species per m^3 of air.

Mathematically, most of the variance is explained by the nss-sulfate values due to their extra weight in the equation to calculate nss-sulfate, but also because nss-sulfate values were significantly higher than nitrate values. Non-sea

salt sulfate also shows a similar bimodal pattern as the primary analytes, though with higher relative peaks in the equatorial Pacific. This matches regional transportation patterns, with higher transport being found in the westerlies of the northern temperate Pacific and the trade winds of the tropical Pacific.

While the equation for calculating acidity presented here has been used previously (Buck et al., 2006) and does show the primary components of acidity, there are other methods to calculate acidity of aerosols (Baker et al., 2021; Mukherjee et al., 2021) that include additional parameters. Some of these methods involve the use of other analytes not measured here, such as organic acid and base pairs (oxalate, methyl sulfonic acid, and a series of simple carboxylic acids), ammonia / ammonium, and chloride depletion. Others use complex modeling with a variety of inputs, including thermodynamic data, charge balance, oxidative state of the atmosphere, and precursor concentrations (Hamilton et al., 2019; Hennigan et al., 2015; Nault et al., 2021) not measured here. These may be more useful in the relatively pristine environment of

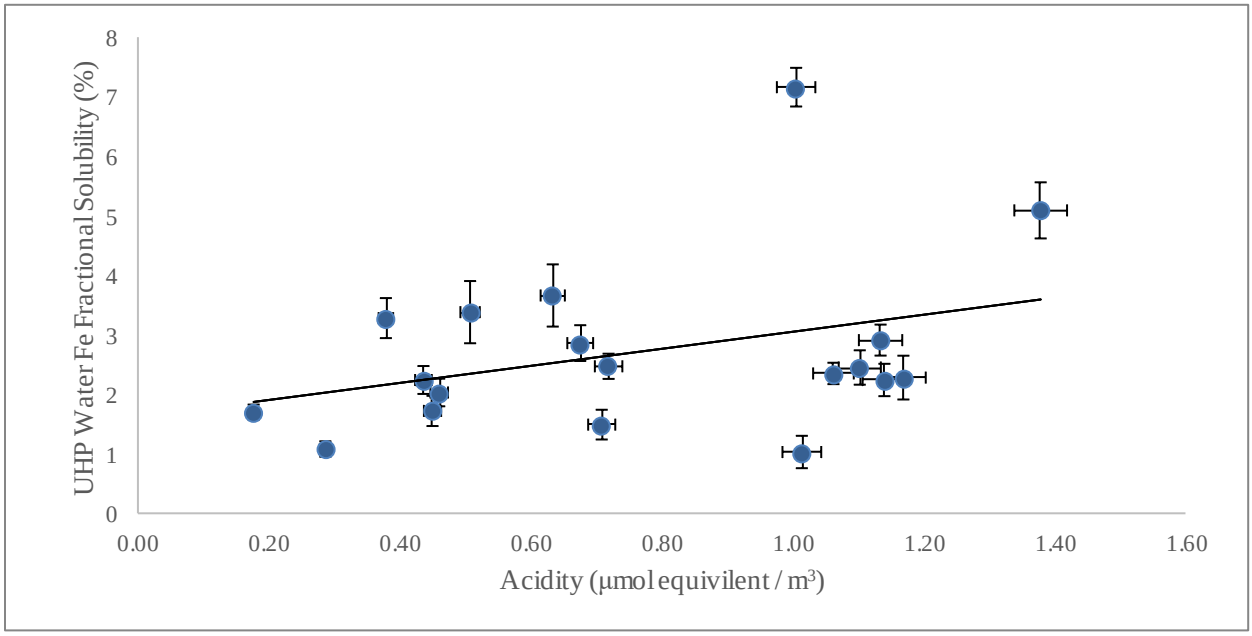

Figure 14 Correlation between UHP Water Fe Fractional Solubility and Acidity in Aerosols. Error bars for acidity are given in Figure 13. Vertical errors are from the propagation of error of the total leach Fe and the UHP Water Fe DI concentrations.

the remote North Pacific, where anthropogenic influence has farther to travel and is more dilute than other sampling locations.

$$\text{Eq 4: } Fe\ \%\ Solubility = \frac{[Fe]_{UHP}}{[Fe]_T} * 100\%$$

Equation 4 was used to calculate the fractional solubility of iron in UHP (hereafter Fe % solubility). The total aerosol Fe data is publicly available (BCO-DMO Project 833916; Marsay et al., 2022). The soluble aerosol Fe ($[Fe]_{UHP}$) is the measured concentration of UHP-soluble iron, while $[Fe]_T$ is the total iron from the complete digests of aerosol bulk samples.

Fe % solubility presented in Figure 14 has a weak ($R^2 = 0.12$, non-significant) relationship with aerosol acidity. This data excludes station 3 because of an order of magnitude difference in ultrapure water iron solubility at that station that may indicate sample contamination. This weak correlation is not supporting of the idea that acidity is the major driving factor in aerosol iron solubility in this region during the low dust season. It is not, however, entirely inconsistent with literature values (Buck et al., 2006) of the relationship in the North Pacific. There are known other processes (particle size, trace gas reactions, photochemistry, wash-out) that influence the relationship between iron fractional solubility, and the relative importance of these processes depends on a great deal of environmental conditions.

Aerosol size is known to be a control on ability for particles to interact with seawater and rainwater due to surface area differences. Course- and fine-mode aerosol size fractions react differently to being exposed to acidity due to the differences in surface area-to-volume ratios. Globally, fine particles are also generally from different sources, especially pyrogenic and gas condensation sources (Ito et al., 2019). Larger particles fall out of the atmosphere faster due to gravity, so samples taken far from the particle sources (such as this study area) are biased towards fine, more soluble particles, regardless of their acidity. Likewise, areas of low average

wind speed (such as the subtropical high-pressure zone) will have larger aerosols fall out of the atmosphere faster than areas of high average wind speed. This sorts aerosols by size differently in specific areas of the sampling transect with different wind regimes thus creating bias towards separate sizes in specific areas of the transect (Chamley, 1989).

Aerosol trace element concentrations were also noted to be "some of the lowest documented during GEOTRACES sampling campaigns" (Marsay et al., 2022). Because of the overall low aerosol concentrations and the extreme distance of transport (as seen in the back-trajectories; Figure 6), the aerosol iron collected in this sampling had already undergone significant atmospheric processing (e.g., cloud formation cycling, trace gas reactions) well before collection. Because of this, assumed associations (such as the association between Fe % solubility and acidity) may be lost prior to collection by other atmospheric processes, especially wash-out of soluble species (of all analytes including iron) by wet deposition in the ITCZ and the stormy GoA.

Lastly, the acidity calculations here, as mentioned prior, are not the only method to calculate acidity as a proxy. Other methods that use more variables (such as ammonia and ammonium ratios, organic acid concentrations, and mineral acid and base) may be more sensitive to the conditions found in the remote areas of the North Pacific during the low-dust portion of the year. Chloride depletion is one of these variables that has been added to this equation in literature (Mukherjee et al., 2021). Chloride depletion in many of the samples overwhelms the acidity calculated here for those samples. Thus, while nss-sulfate and nitrate may dominate the acidity of most aerosol samples, there may be other factors that become important at the low total concentrations found in the remote areas of the ocean. Chloride depletion is also not a linear process and depends on the interaction of chloride with sulfuric acid in aerosol particles which

changes for particle size, shape, and origin (McInnes et al., 1994; Zhao & Gao, 2008). Likewise, the HCl liberated during this process is commonly deposited as dry deposition downwind, which complicates the variable's use as a contributor to acidity calculations (McInnes et al., 1994; Ten Harkel, 1997; Zhao & Gao, 2008).

Other studies have attempted to compare some proxy of acid forming species (typically nss-sulfate) and DI Fe fractional solubility (Buck et al., 2006; Hsu et al., 2014; Kumar et al., 2010). These different sampling campaigns took place in a variety of different regimes downwind from Asia. Hsu et al (2014) sampled the South China Sea, largely between the Philippines and Indonesia in a highly anthropogenically influenced area. This study also noted multiple biomass burning events upwind from collection and showed a robust relationship between iron fractional solubility and nss-sulfate concentrations. Kumar et al (2010) collected aerosols in the Bay of Bengal and had two distinct atmospheric origin patterns. The samples that were taken downwind from the Indo-Gangetic plain (a densely populated, industrialized area) had a significant relationship ($R^2 = 0.56$) between nss-sulfate and DI iron fractional solubility. However, the samples taken in the southern Bay of Bengal (largely influenced by marine air and the mountain ranges of Southeast Asia) had a poor correlation between nss-sulfate and DI iron fractional solubility. Lastly, Buck et al (2006) crossed the West Pacific Ocean, between Japan and Hawaii, initially following the Kuroshio Current before sailing southward toward the Hawaiian Islands. This cruise also noted poor correlation between calculated aerosol acidity and aerosol iron fractional solubility in deionized water.

Among these sampling efforts, a trend emerges. The samples that were taken downwind from major population centers and/or biomass burnings show a stronger correlation between nss-sulfate or acidity and iron fractional solubility. Meanwhile, the samples that were taken in remote

or pristine areas of the ocean, with aerosols farther from anthropogenic influence, have a much weaker (if any) correlation. This matches the findings found in this paper, where there was low correlation found in the remote Northeast Pacific. This pattern suggests that the correlation between acidity and iron fractional solubility is due to the high nss-sulfate aerosol sources themselves having higher fractional iron solubility. More research is required on aerosol chemistry to understand the role in atmospheric transport and processing of aerosols on fractional solubility.

CHAPTER 4

CONCLUSION

These data show a weak relationship between aerosol iron fractional solubility and acidity, as measured by nss-sulfate and nitrate in the study area. Questions remain as to what processes drive the solubility differences in aerosol iron, including aerosol particle size (Hsieh et al., 2022), CCN chemical reactions (Fan et al., 2004; Shi et al., 2009; Shi et al., 2015), gas-solid phase interactions, microlayer chemistry (Barker & Zeitlin, 1972; Hardy et al., 1985), and aerosol origins (Hsu et al., 2014; Kumar et al., 2010). Parameterizing these processes and how each impacts aerosol iron solubility should be a focus for future research into the drivers of differences in solubility of aerosol trace elements. Those solubility differences are important to understanding the primary production in the iron limited sectors of the open ocean. These data also suggest that the major global wind patterns are the primary drivers of aerosol concentration in this portion of the world.

Because of predictions of increased ocean stratification, aerosol deposition is becoming an increasingly important variable in models of marine primary production. Dust deposition has been hypothesized to be a major control on primary production through geological time in the equatorial Pacific (Costa et al., 2016; Winckler et al., 2016) especially during times of high mineral loading. Some studies have suggested that dust dynamics may also cause secondary effects by increasing nutrient usage in downwelling subantarctic water parcels, preventing that nutrient usage elsewhere and influencing global nitrogen and phosphorus cycles through primary production changes (Winckler et al., 2016). By influencing primary production, aerosol

deposition of these limiting metals plays a significant role in the carbon cycle and climate. As the global climate continues to change and anthropogenic influence continues to increase, aerosol composition and fluxes will be altered (Guo et al., 2019). Understanding these changes and how they will affect the amount of bioavailable trace elements reaching the ocean is a vital insight into the future of carbon cycling, nutrient cycling, and primary productivity in the Pacific Ocean and beyond.

REFERENCES

Alves, C. A., Gonçalves, C., Pio, C. A., Mirante, F., Caseiro, A., Tarelho, L., Freitas, M. C., & Viegas, D. X. (2010). Smoke emissions from biomass burning in a Mediterranean shrubland. *Atmospheric Environment*, *44*(25), 3024-3033. https://doi.org/10.1016/j.atmosenv.2010.05.010

Amor, M., Tharaud, M., Gélabert, A., & Komeili, A. (2020). Single-cell determination of iron content in magnetotactic bacteria: implications for the iron biogeochemical cycle. *Environmental Microbiology*, *22*(3), 823-831. https://doi.org/10.1111/1462-2920.14708

Baker, A. R., & Croot, P. L. (2010). Atmospheric and marine controls on aerosol iron solubility in seawater. *Marine Chemistry*, *120*(1-4), 4-13. https://doi.org/10.1016/j.marchem.2008.09.003

Baker, A. R., Kanakidou, M., Nenes, A., Myriokefalitakis, S., Croot, P. L., Duce, R. A., Gao, Y., Guieu, C., Ito, A., Jickells, T. D., Mahowald, N. M., Middag, R., Perron, M. M. G., Sarin, M. M., Shelley, R., & Turner, D. R. (2021). Changing atmospheric acidity as a modulator of nutrient deposition and ocean biogeochemistry. *Science Advances*, *7*(28), eabd8800. https://doi.org/10.1126/sciadv.abd8800

Barker, D. R., & Zeitlin, H. (1972). Metal-ion concentrations in sea-surface microlayer and size-separated atmospheric aerosol samples in Hawaii. *Journal of Geophysical Research*, *77*(27), 5076-5086. https://doi.org/10.1029/jc077i027p05076

Buck, C. S., Aguilar-Islas, A., Marsay, C., Kadko, D., & Landing, W. M. (2019). Trace element concentrations, elemental ratios, and enrichment factors observed in aerosol samples collected during the US GEOTRACES eastern Pacific Ocean transect (GP16). *Chemical Geology*, *511*, 212-224. https://doi.org/10.1016/j.chemgeo.2019.01.002

Buck, C. S., Landing, W. M., & Resing, J. (2013). Pacific Ocean aerosols: Deposition and solubility of iron, aluminum, and other trace elements. *Marine Chemistry*, *157*, 117-130. https://doi.org/10.1016/j.marchem.2013.09.005

Buck, C. S., Landing, W. M., Resing, J. A., & Lebon, G. T. (2006). Aerosol iron and aluminum solubility in the northwest Pacific Ocean: Results from the 2002 IOC cruise. *Geochemistry, Geophysics, Geosystems*, *7*(4), n/a-n/a. https://doi.org/10.1029/2005gc000977

Buck, C. S., Landing, W. M., Resing, J. A., & Measures, C. I. (2010). The solubility and deposition of aerosol Fe and other trace elements in the North Atlantic Ocean: Observations from the A16N CLIVAR/CO2 repeat hydrography section. *Marine Chemistry*, *120*(1-4), 57-70. https://doi.org/10.1016/j.marchem.2008.08.003

Chamley, H. (1989). Aeolian Input. In *Clay Sedimentology* (pp. 133-161). Springer Berlin Heidelberg. https://doi.org/10.1007/978-3-642-85916-8_7

Chen, H., Navea, J. G., Young, M. A., & Grassian, V. H. (2011). Heterogeneous Photochemistry of Trace Atmospheric Gases with Components of Mineral Dust

Aerosol. *The Journal of Physical Chemistry A*, *115*(4), 490-499. https://doi.org/10.1021/jp110164j

Chester, R., Murphy, K. J. T., Lin, F. J., Berry, A. S., Bradshaw, G. A., & Corcoran, P. A. (1993). Factors controlling the solubilities of trace metals from non-remote aerosols deposited to the sea surface by the 'dry' deposition mode. *Marine Chemistry*, *42*(2), 107-126. https://doi.org/10.1016/0304-4203(93)90241-f

Conway, T. M., Hamilton, D. S., Shelley, R. U., Aguilar-Islas, A. M., Landing, W. M., Mahowald, N. M., & John, S. G. (2019). Tracing and constraining anthropogenic aerosol iron fluxes to the North Atlantic Ocean using iron isotopes. *Nature Communications*, *10*(1). https://doi.org/10.1038/s41467-019-10457-w

Costa, K. M., McManus, J. F., Anderson, R. F., Ren, H., Sigman, D. M., Winckler, G., Fleisher, M. Q., Marcantonio, F., & Ravelo, A. C. (2016). No iron fertilization in the equatorial Pacific Ocean during the last ice age. *Nature*, *529*(7587), 519-522. https://doi.org/10.1038/nature16453

Coyle, K. O., Hermann, A. J., & Hopcroft, R. R. (2019). Modeled spatial-temporal distribution of productivity, chlorophyll, iron and nitrate on the northern Gulf of Alaska shelf relative to field observations. *Deep Sea Research Part II: Topical Studies in Oceanography*, *165*, 163-191. https://doi.org/10.1016/j.dsr2.2019.05.006

Dai, Y., Cao, L., & Wang, B. (2019). Marine biogeochemical cycling and oceanic CO2 uptake simulated by the NUIST Earth System Model version 3. *Geoscientific Model Development Discussions*, *2019*, 1-55.

Damle, A. S., Ensor, D. S., & Ranade, M. B. (1981). Coal Combustion Aerosol Formation Mechanisms: A Review. *Aerosol Science and Technology*, *1*(1), 119-133. https://doi.org/10.1080/02786828208958582

de Baar, H. J., Buma, A. G., Nolting, R. F., Cadée, G. C., Jacques, G., & Tréguer, P. J. (1990). On iron limitation of the Southern Ocean: experimental observations in the Weddell and Scotia Seas. *Marine ecology progress series*, 105-122.

Duce, R. A., & Tindale, N. W. (1991). Atmospheric transport of iron and its deposition in the ocean. *Limnology and Oceanography*, *36*(8), 1715-1726. https://doi.org/10.4319/lo.1991.36.8.1715

Echalar, F., Gaudichet, A., Cachier, H., & Artaxo, P. (1995). Aerosol emissions by tropical forest and savanna biomass burning: Characteristic trace elements and fluxes. *Geophysical Research Letters*, *22*(22), 3039-3042. https://doi.org/10.1029/95gl03170

Fan, S.-M., Horowitz, L. W., Levy, H., & Moxim, W. J. (2004). Impact of air pollution on wet deposition of mineral dust aerosols. *Geophysical Research Letters*, *31*(2), n/a-n/a. https://doi.org/10.1029/2003gl018501

Fitzgerald, J. W. (1991). Marine aerosols: A review. *Atmospheric Environment. Part A. General Topics*, *25*(3-4), 533-545. https://doi.org/10.1016/0960-1686(91)90050-h

Fung, I. Y., Meyn, S. K., Tegen, I., Doney, S. C., John, J. G., & Bishop, J. K. B. (2000). Iron supply and demand in the upper ocean. *Global Biogeochemical Cycles*, *14*(1), 281-295. https://doi.org/10.1029/1999gb900059

Ghahremaninezhad, R., Norman, A.-L., Abbatt, J. P. D., Levasseur, M., & Thomas, J. L. (2016). Biogenic, anthropogenic and sea salt sulfate size-segregated aerosols in

the Arctic summer. *Atmospheric Chemistry and Physics*, *16*(8), 5191-5202. https://doi.org/10.5194/acp-16-5191-2016

Ghan, S. J. (2013). Technical Note: Estimating aerosol effects on cloud radiative forcing. *Atmospheric Chemistry and Physics*, *13*(19), 9971-9974. https://doi.org/10.5194/acp-13-9971-2013

Ginoux, P., Chin, M., Tegen, I., Prospero, J. M., Holben, B., Dubovik, O., & Lin, S.-J. (2001). Sources and distributions of dust aerosols simulated with the GOCART model. *Journal of Geophysical Research: Atmospheres*, *106*(D17), 20255-20273. https://doi.org/10.1029/2000jd000053

Guo, J., Xu, H., Liu, L., Chen, D., Peng, Y., Yim, S. H. L., Yang, Y., Li, J., Zhao, C., & Zhai, P. (2019). The Trend Reversal of Dust Aerosol Over East Asia and the North Pacific Ocean Attributed to Large-Scale Meteorology, Deposition, and Soil Moisture. *Journal of Geophysical Research: Atmospheres*, *124*(19), 10450-10466. https://doi.org/10.1029/2019jd030654

Hamilton, D. S., Moore, J. K., Arneth, A., Bond, T. C., Carslaw, K. S., Hantson, S., Ito, A., Kaplan, J. O., Lindsay, K., Nieradzik, L., Rathod, S. D., Scanza, R. A., & Mahowald, N. M. (2020). Impact of Changes to the Atmospheric Soluble Iron Deposition Flux on Ocean Biogeochemical Cycles in the Anthropocene. *Global Biogeochemical Cycles*, *34*(3). https://doi.org/10.1029/2019gb006448

Hamilton, D. S., Scanza, R. A., Feng, Y., Guinness, J., Kok, J. F., Li, L., Liu, X., Rathod, S. D., Wan, J. S., Wu, M., & Mahowald, N. M. (2019). Improved methodologies for Earth system modelling of atmospheric soluble iron and observation comparisons using the Mechanism of Intermediate complexity for Modelling Iron (MIMI v1.0). *Geoscientific Model Development*, *12*(9), 3835-3862. https://doi.org/10.5194/gmd-12-3835-2019

Hand, J. L. (2004). Estimates of atmospheric-processed soluble iron from observations and a global mineral aerosol model: Biogeochemical implications. *Journal of Geophysical Research*, *109*(D17). https://doi.org/10.1029/2004jd004574

Hardy, J. T., Apts, C. W., Crecelius, E. A., & Fellingham, G. W. (1985). The sea-surface microlayer: Fate and residence times of atmospheric metals1. *Limnology and Oceanography*, *30*(1), 93-101. https://doi.org/10.4319/lo.1985.30.1.0093

Hennigan, C. J., Izumi, J., Sullivan, A. P., Weber, R. J., & Nenes, A. (2015). A critical evaluation of proxy methods used to estimate the acidity of atmospheric particles. *Atmospheric Chemistry and Physics*, *15*(5), 2775-2790. https://doi.org/10.5194/acp-15-2775-2015

Hinckley, S., Coyle, K. O., Gibson, G., Hermann, A. J., & Dobbins, E. L. (2009). A biophysical NPZ model with iron for the Gulf of Alaska: Reproducing the differences between an oceanic HNLC ecosystem and a classical northern temperate shelf ecosystem. *Deep Sea Research Part II: Topical Studies in Oceanography*, *56*(24), 2520-2536. https://doi.org/10.1016/j.dsr2.2009.03.003

Hsieh, C.-C., Chen, H.-Y., & Ho, T.-Y. (2022). The effect of aerosol size on Fe solubility and deposition flux: A case study in the East China Sea. *Marine Chemistry*, *241*, 104106. https://doi.org/10.1016/j.marchem.2022.104106

Hsu, S. C., Gong, G. C., Shiah, F. K., Hung, C. C., Kao, S. J., Zhang, R., Chen, W. N., Chen, C. C., Chou, C. C. K., Lin, Y. C., Lin, F. J., & Lin, S. H. (2014). *Sources, solubility, and acid processing of aerosol iron and phosphorous over the South*

China Sea: East Asian dust and pollution outflows vs. Southeast Asian biomass burning. Copernicus GmbH. https://dx.doi.org/10.5194/acpd-14-21433-2014

Hutchins, D., & Bruland, K. (1994). Grazer-mediated regeneration and assimilation of Fe, Zn and Mn from planktonic prey. *Marine Ecology-Progress Series*, *110*, 259-259.

Hutchins, D. A., Witter, A. E., Butler, A., & Luther, G. W. (1999). Competition among marine phytoplankton for different chelated iron species. *Nature*, *400*(6747), 858-861. https://doi.org/10.1038/23680

IPCC. (2021). *IPCC Action Report 6*.

Ito, A., Myriokefalitakis, S., Kanakidou, M., Mahowald, N. M., Scanza, R. A., Hamilton, D. S., Baker, A. R., Jickells, T., Sarin, M., Bikkina, S., Gao, Y., Shelley, R. U., Buck, C. S., Landing, W. M., Bowie, A. R., Perron, M. M. G., Guieu, C., Meskhidze, N., Johnson, M. S., . . . Duce, R. A. (2019). Pyrogenic iron: The missing link to high iron solubility in aerosols. *Science Advances*, *5*(5), eaau7671. https://doi.org/doi:10.1126/sciadv.aau7671

Ito, A., & Shi, Z. (2016). Delivery of anthropogenic bioavailable iron from mineral dust and combustion aerosols to the ocean. *Atmospheric Chemistry and Physics*, *16*(1), 85-99. https://doi.org/10.5194/acp-16-85-2016

Kelly, R. L., Bian, X., Feakins, S. J., Fornace, K. L., Gunderson, T., Hawco, N. J., Liang, H., Niggemann, J., Paulson, S. E., Pinedo-Gonzalez, P., West, A. J., Yang, S. C., & John, S. G. (2021). Delivery of Metals and Dissolved Black Carbon to the Southern California Coastal Ocean via Aerosols and Floodwaters Following the 2017 Thomas Fire. *Journal of Geophysical Research: Biogeosciences*, *126*(3). https://doi.org/10.1029/2020jg006117

Kessler, N., Armoza-Zvuloni, R., Wang, S., Basu, S., Weber, P. K., Stuart, R. K., & Shaked, Y. (2020). Selective collection of iron-rich dust particles by natural Trichodesmium colonies. *The ISME Journal*, *14*(1), 91-103. https://doi.org/10.1038/s41396-019-0505-x

Kok, J. F., Ward, D. S., Mahowald, N. M., & Evan, A. T. (2018). Global and regional importance of the direct dust-climate feedback. *Nature Communications*, *9*(1). https://doi.org/10.1038/s41467-017-02620-y

Kolber, Z. S., Barber, R. T., Coale, K. H., Fitzwateri, S. E., Greene, R. M., Johnson, K. S., Lindley, S., & Falkowski, P. G. (1994). Iron limitation of phytoplankton photosynthesis in the equatorial Pacific Ocean. *Nature*, *371*(6493), 145-149.

Kumar, A., Sarin, M. M., & Srinivas, B. (2010). Aerosol iron solubility over Bay of Bengal: Role of anthropogenic sources and chemical processing. *Marine Chemistry*, *121*(1-4), 167-175. https://doi.org/10.1016/j.marchem.2010.04.005

Labatut, M., Lacan, F., Pradoux, C., Chmeleff, J., Radic, A., Murray, J. W., Poitrasson, F., Johansen, A. M., & Thil, F. (2014). Iron sources and dissolved-particulate interactions in the seawater of the Western Equatorial Pacific, iron isotope perspectives. *Global Biogeochemical Cycles*, *28*(10), 1044-1065. https://doi.org/10.1002/2014gb004928

Li, W., Xu, L., Liu, X., Zhang, J., Lin, Y., Yao, X., Gao, H., Zhang, D., Chen, J., & Wang, W. (2017). Air pollution–aerosol interactions produce more bioavailable iron for ocean ecosystems. *Science Advances*, *3*(3), e1601749.

Mahowald, N. M., Baker, A. R., Bergametti, G., Brooks, N., Duce, R. A., Jickells, T. D., Kubilay, N., Prospero, J. M., & Tegen, I. (2005). Atmospheric global dust cycle and iron inputs to the ocean. *Global Biogeochemical Cycles*, *19*(4), n/a-n/a. https://doi.org/10.1029/2004gb002402

Marsay, C. M., Kadko, D., Landing, W. M., & Buck, C. S. (2022). Bulk aerosol trace element concentrations and deposition fluxes during the US GEOTRACES GP15 Pacific Meridional Transect. *Global Biogeochemical Cycles*. https://doi.org/10.1029/2021gb007122

Martin, J. H., & Fitzwater, S. E. (1988). Iron deficiency limits phytoplankton growth in the north-east Pacific subarctic. *Nature*, *331*(6154), 341-343.

McInnes, L., Covert, D., Quinn, P., & Germani, M. (1994). Measurements of chloride depletion and sulfur enrichment in individual sea-salt particles collected from the remote marine boundary layer. *Journal of Geophysical Research: Atmospheres*, *99*(D4), 8257-8268.

Moore, C. M., Mills, M. M., Arrigo, K. R., Berman-Frank, I., Bopp, L., Boyd, P. W., Galbraith, E. D., Geider, R. J., Guieu, C., Jaccard, S. L., Jickells, T. D., La Roche, J., Lenton, T. M., Mahowald, N. M., Marañón, E., Marinov, I., Moore, J. K., Nakatsuka, T., Oschlies, A., . . . Ulloa, O. (2013). Processes and patterns of oceanic nutrient limitation. *Nature Geoscience*, *6*(9), 701-710. https://doi.org/10.1038/ngeo1765

Morton, P. L., Landing, W. M., Hsu, S.-C., Milne, A., Aguilar-Islas, A. M., Baker, A. R., Bowie, A. R., Buck, C. S., Gao, Y., Gichuki, S., Hastings, M. G., Hatta, M., Johansen, A. M., Losno, R., Mead, C., Patey, M. D., Swarr, G., Vandermark, A., & Zamora, L. M. (2013). Methods for the sampling and analysis of marine aerosols: results from the 2008 GEOTRACES aerosol intercalibration experiment. *Limnology and Oceanography: Methods*, *11*(2), 62-78. https://doi.org/10.4319/lom.2013.11.62

Mukherjee, P., Marsay, C. M., Yu, S., Buck, C. S., Landing, W. M., & Gao, Y. (2021). Concentrations and size-distributions of water-soluble inorganic and organic species on aerosols over the Arctic Ocean observed during the US GEOTRACES Western Arctic Cruise GN01. *Atmospheric Environment*, *261*, 118569. https://doi.org/10.1016/j.atmosenv.2021.118569

Nault, B. A., Campuzano-Jost, P., Day, D. A., Jo, D. S., Schroder, J. C., Allen, H. M., Bahreini, R., Bian, H., Blake, D. R., Chin, M., Clegg, S. L., Colarco, P. R., Crounse, J. D., Cubison, M. J., Decarlo, P. F., Dibb, J. E., Diskin, G. S., Hodzic, A., Hu, W., . . . Jimenez, J. L. (2021). Chemical transport models often underestimate inorganic aerosol acidity in remote regions of the atmosphere. *Communications Earth & Environment*, *2*(1). https://doi.org/10.1038/s43247-021-00164-0

Paris, R., & Desboeufs, K. V. (2013). Effect of atmospheric organic complexation on iron-bearing dust solubility. *Atmospheric Chemistry and Physics*, *13*(9), 4895-4905. https://doi.org/10.5194/acp-13-4895-2013

Pavia, F. J., Anderson, R. F., Winckler, G., & Fleisher, M. Q. (2020). Atmospheric Dust Inputs, Iron Cycling, and Biogeochemical Connections in the South Pacific Ocean From Thorium Isotopes. *Global Biogeochemical Cycles*, *34*(9). https://doi.org/10.1029/2020gb006562

Perron, M. M. G., Strzelec, M., Gault-Ringold, M., Proemse, B. C., Boyd, P. W., & Bowie, A. R. (2020). Assessment of leaching protocols to determine the solubility of trace metals in aerosols. *Talanta*, *208*, 120377. https://doi.org/10.1016/j.talanta.2019.120377

Pinedo-González, P., Hawco, N. J., Bundy, R. M., Armbrust, E. V., Follows, M. J., Cael, B. B., White, A. E., Ferrón, S., Karl, D. M., & John, S. G. (2020). Anthropogenic Asian aerosols provide Fe to the North Pacific Ocean. *Proceedings of the National Academy of Sciences*, *117*(45), 27862-27868. https://doi.org/10.1073/pnas.2010315117

Rolph, G., Stein, A., & Stunder, B. (2017). Real-time Environmental Applications and Display sYstem: READY. *Environmental Modelling & Software*, *95*, 210-228. https://doi.org/10.1016/j.envsoft.2017.06.025

Schepanski, K. (2018). Transport of Mineral Dust and Its Impact on Climate. *Geosciences*, *8*(5), 151. https://doi.org/10.3390/geosciences8050151

SCOR. (2007). GEOTRACES – An international study of the global marine biogeochemical cycles of trace elements and their isotopes. *Geochemistry*, *67*(2), 85-131. https://doi.org/10.1016/j.chemer.2007.02.001

Shaked, Y., & Lis, H. (2012). Disassembling Iron Availability to Phytoplankton [Review]. *Frontiers in microbiology*, *3*. https://doi.org/10.3389/fmicb.2012.00123

Shi, Z., Krom, M. D., Bonneville, S., Baker, A. R., Jickells, T. D., & Benning, L. G. (2009). Formation of Iron Nanoparticles and Increase in Iron Reactivity in Mineral Dust during Simulated Cloud Processing. *Environmental Science & Technology*, *43*(17), 6592-6596. https://doi.org/10.1021/es901294g

Shi, Z., Krom, M. D., Bonneville, S., & Benning, L. G. (2015). Atmospheric Processing Outside Clouds Increases Soluble Iron in Mineral Dust. *Environmental Science & Technology*, *49*(3), 1472-1477. https://doi.org/10.1021/es504623x

Sholkovitz, E. R., Sedwick, P. N., Church, T. M., Baker, A. R., & Powell, C. F. (2012). Fractional solubility of aerosol iron: Synthesis of a global-scale data set. *Geochimica et Cosmochimica Acta*, *89*, 173-189. https://doi.org/10.1016/j.gca.2012.04.022

Spokes, L. J., & Jickells, T. D. (1995). Factors controlling the solubility of aerosol trace metals in the atmosphere and on mixing into seawater. *Aquatic Geochemistry*, *1*(4), 355-374. https://doi.org/10.1007/BF00702739

Stein, A. F., Draxler, R. R., Rolph, G. D., Stunder, B. J. B., Cohen, M. D., & Ngan, F. (2015). NOAA's HYSPLIT Atmospheric Transport and Dispersion Modeling System. *Bulletin of the American Meteorological Society*, *96*(12), 2059-2077. https://doi.org/10.1175/bams-d-14-00110.1

Stewart, C., Johnston, D. M., Leonard, G. S., Horwell, C. J., Thordarson, T., & Cronin, S. J. (2006). Contamination of water supplies by volcanic ashfall: A literature review and simple impact modelling. *Journal of Volcanology and Geothermal Research*, *158*(3-4), 296-306. https://doi.org/10.1016/j.jvolgeores.2006.07.002

Sutak, R., Camadro, J.-M., & Lesuisse, E. (2020). Iron uptake mechanisms in marine phytoplankton. *Frontiers in microbiology*, 2831.

Tagliabue, A., Bowie, A. R., Boyd, P. W., Buck, K. N., Johnson, K. S., & Saito, M. A. (2017). The integral role of iron in ocean biogeochemistry. *Nature*, *543*(7643), 51-59. https://doi.org/10.1038/nature21058

Taylor, S. R., & McLennan, S. M. (1995). The geochemical evolution of the continental crust. *Reviews of Geophysics*, *33*(2), 241. https://doi.org/10.1029/95rg00262

Ten Harkel, M. (1997). The effects of particle-size distribution and chloride depletion of sea-salt aerosols on estimating atmospheric deposition at a coastal site. *Atmospheric Environment*, *31*(3), 417-427.

Wang, C. (2013). Impact of anthropogenic absorbing aerosols on clouds and precipitation: A review of recent progresses. *Atmospheric Research*, *122*, 237-249. https://doi.org/10.1016/j.atmosres.2012.11.005

Winckler, G., Anderson, R. F., Jaccard, S. L., & Marcantonio, F. (2016). Ocean dynamics, not dust, have controlled equatorial Pacific productivity over the past 500,000 years. *Proceedings of the National Academy of Sciences*, *113*(22), 6119-6124. https://doi.org/10.1073/pnas.1600616113

Zender, C. S. (2003). Mineral Dust Entrainment and Deposition (DEAD) model: Description and 1990s dust climatology. *Journal of Geophysical Research*, *108*(D14). https://doi.org/10.1029/2002jd002775

Zhao, T. L., Gong, S. L., Zhang, X. Y., Blanchet, J. P., McKendry, I. G., & Zhou, Z. J. (2006). A Simulated Climatology of Asian Dust Aerosol and Its Trans-Pacific Transport. Part I: Mean Climate and Validation. *Journal of Climate*, *19*(1), 88-103. https://doi.org/10.1175/jcli3605.1

Zhao, Y., & Gao, Y. (2008). Acidic species and chloride depletion in coarse aerosol particles in the US east coast. *Science of The Total Environment*, *407*(1), 541-547.